Journal of Alloys and Compounds 502 (2010) 199–205

Contents lists available at ScienceDirect

Journal of Alloys and Compounds

journal homepage: www.elsevier.com/locate/jallcom

Polyol synthesis of (polyvinylpyrrolidone) PVP–Mn_3O_4 nanocomposite

A. Baykal[a,*], N. Bıtrak[a], B. Ünal[b], H. Kavas[b], Z. Durmus[a], Ş. Özden[a], M.S. Toprak[c]

[a] Department of Chemistry, Fatih University, B.Çekmece, 34500 Istanbul, Turkey
[b] Department of Physics, Fatih University, B.Çekmece, 34500 Istanbul, Turkey
[c] Functional Materials Division, Royal Institute of Technology – KTH, SE-16440 Stockholm, Sweden

ARTICLE INFO

Article history:
Received 8 January 2010
Received in revised form 15 April 2010
Accepted 20 April 2010
Available online 15 May 2010

Keywords:
Nanocomposite
Nanomagnetic materials
ac conductivity
Magnetization

ABSTRACT

We report on the synthesis of (polyvinylpyrrolidone) PVP–Mn_3O_4 nanocomposite via a polyol route. Crystalline phase was identified as Mn_3O_4 and the crystallite size was obtained as 6 ± 1 nm from X-ray line profile fitting. Average particle size of 6.1 ± 0.1 nm obtained from TEM analysis reveals nearly single crystalline nature of these nanoparticles in the composite. The capping of PVP around Mn_3O_4 nanoparticles was confirmed by FT-IR spectroscopy, the interaction being via bridging oxygens of the carbonyl (C=O) and the nanoparticle surface. T_C and T_B for PVP–Mn_3O_4 nanocomposite were observed at 42 K and 28.5 K, respectively. The sample has hysteresis with small coercivity and remanent magnetization at 40 K, resembling the superparamagnetic state. ac conductivity measurements on PVP–Mn_3O_4 nanocomposite revealed a conductivity in the order of 10^{-7} S cm^{-1} at lower frequencies. The conductivity change with respect to frequency can be explained by electronic exchange occurring between Mn^{+2} and Mn^{+3} existing in sublattice of spinel lattice.

1. Introduction

Transition-metal oxide nanoparticles can exhibit enhanced optical, magnetic and electrical properties as compared to their bulk counterparts, rendering such nanoparticles interesting for a variety of applications [1,2]. Among magnetic nanoparticles, manganese oxide (Mn_3O_4) as a magnetic transition-metal oxide is an important material. It has a wide range of applications as catalyst, ion-exchange medium, molecular adsorbent, and in electrochemical materials and varistors [3–7]. Furthermore, Mn_3O_4 has been widely used as the main source of ferrite materials, finding extensive applications in electronics and information technologies. Mn_3O_4 is known to crystallize in the normal spinel structure with a tetragonal distortion elongated along the *c*-axis. Manganese ions are placed in the tetrahedral A-sites (Mn^{2+}) and octahedral B-sites (Mn^{3+}).

In the literature, there are many diverse methods to prepare Mn_3O_4 nanoparticles including chemical bath deposition [8], solvothermal [9], coprecipitation [10], microwave irradiation [11,12], and surfactant-assisted methods [13], which are interesting and attract much research attention. However, these preparation methods are generally complicated and complex process controls are involved. Furthermore, agglomeration and wide particle size distribution are the drawbacks associated with most of these methods. On the other hand, polyol process [14,15] is a versatile chemical approach, which uses poly alcohols (ethylene glycol, diethylene glycol) to reduce metal salts to metal particles, was successfully used to prepare a great variety of non-aggregated inorganic compounds. The polyols often serve as reaction medium with high boiling point solvent and reducing agent, as well as stabilizer to control the particle growth and prevent interparticle aggregation. The advantage of this method is the possibility to control experimental conditions and easy scale-up [16].

2. Experimental

Manganese acetylacetonate ($Mn(acac)_3$) (Alfa Aesar), 1,2-hexadecanediol ($C_{16}H_{34}O_2$) (ABCR), diethyl ether ($C_{12}H_{10}O$) (Alfa Aesar) and PVP (polyvinyl pyrrolidone) (Merck) used without further purification.

Manganese acetylacetonate ($Mn(acac)_3$), 1,2-hexadecanediol, 20 mL diethyl ether and 0.4 g PVP polymer were mixed and magnetically stirred. Then the mixture was slowly heated to 393 K for 2 h. Afterwards the temperature was rapidly raised to 533 K and refluxed for 2 h to complete the reaction. The PVP–Mn_3O_4 nanocomposite was precipitated, centrifuged and dispersed in hexane without any further modification.

3. Results and discussion

3.1. XRD analysis

X-ray powder diffraction (XRD) analysis was conducted on a Rigaku Smart Lab Diffractometer operated at 40 kV and 35 mA using Cu Kα radiation. XRD powder pattern of as-synthesized PVP–Mn_3O_4 nanocomposite is presented in Fig. 1. All diffraction

* Corresponding author. Tel.: +90 212 866 33 00x2061; fax: +90 212 866 34 02.
E-mail address: hbaykal@fatih.edu.tr (A. Baykal).

0925-8388/$ – see front matter © 2010 Elsevier B.V. All rights reserved.
doi:10.1016/j.jallcom.2010.04.143

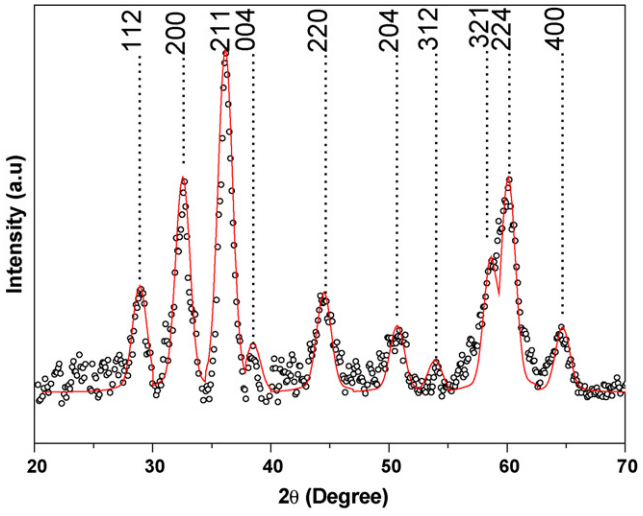

Fig. 1. XRD powder pattern (◦) and line profile fitting (-) of PVP–Mn_3O_4 nanocomposite.

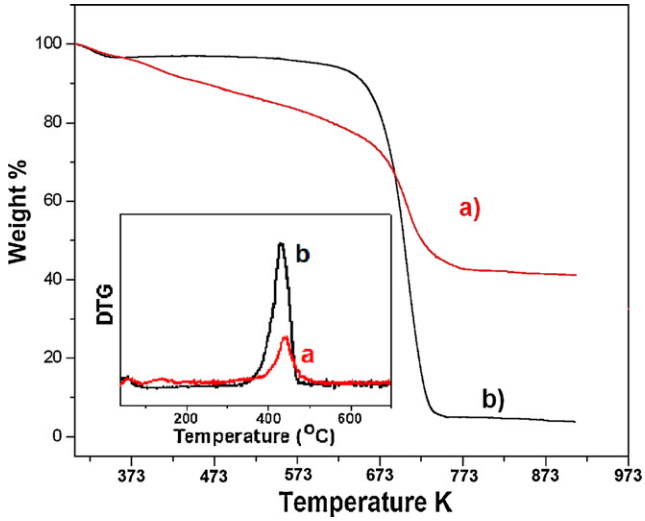

Fig. 3. TGA and differential thermograms of (a) PVP–Mn_3O_4 nanocomposite (b) pure PVP.

peaks were indexed to the tetragonal hausmannite crystal structure model of Mn_3O_4 (which are consistent with bulk value -ICDD Card no. 24-0734). No extra peaks of impurities indicating other forms of manganese oxides were detected. The mean size of the crystallites was estimated from the diffraction pattern using the line profile fitting equation given in Wejrzanowski et al. [17] and Pielaszek [18]. The line profile, shown in Fig. 1, is fitted for 9 peaks (1 1 2), (2 0 0), (2 1 1), (0 0 4), (2 2 0), (2 0 4), (3 1 2), (2 2 4), and (4 0 0). The average crystallite size, D and σ, was estimated as 6 ± 1 nm.

Mn_3O_4 is a mixed oxide containing Mn ions with two different oxidation states; namely +2 and +3. This result suggests that Mn^{2+} ions are produced by the reduction of Mn^{3+} ions during reflux at high temperature which were then used in the formation of Mn_3O_4.

3.2. FT-IR analysis

Fourier transform infrared (FT-IR) spectra were recorded in transmission mode with a PerkinElmer BX FT-IR infrared spectrometer. The powder samples were ground with KBr and compressed into a pellet. FT-IR spectra in the range 4000–400 cm^{-1} were recorded in order to investigate the nature of the chemical bonds formed. Infrared studies were conducted to investigate the type of interaction between Mn_3O_4 nanoparticles and PVP host polymer. The FT-IR spectra of PVP and PVP–Mn_3O_4 nanocomposite are shown in Fig. 2. It is worth noting that the C=O stretch band is present at 1660 cm^{-1} for pure PVP (Fig. 1(a)) and after formation of PVP–Mn_3O_4 nanocomposite this stretching red shifts ~20 cm^{-1}

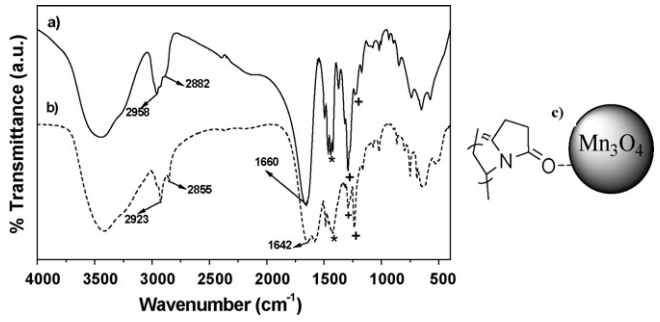

Fig. 2. FT-IR spectra of (a) pure PVP (b) PVP–Mn_3O_4 nanocomposite, and (c) Suggested conjugation scheme of PVP onto Mn_3O_4 nanoparticles. –C–N stretching vibrations and –C–H bending vibrations are indicated with "+" and "*" respectively.

(Fig. 2(b)) indicating a strong interaction between Mn_3O_4 nanoparticles and C=O of PVP host matrix. The asymmetric CH_2 stretch (2952 cm^{-1}) and symmetric CH_2 stretch (2892 cm^{-1}) shifted to 2922 cm^{-1} and 2852 cm^{-1}, respectively. In addition, FT-IR spectra of the particles exhibit characteristic peaks of Mn_3O_4 at around 613 cm^{-1} and 503 cm^{-1}, respectively [4–7,19–21]. For the rest of the peaks, no significant shifts were observed and this suggested that Mn_3O_4 nanoparticles have interaction with PVP through C=O group as schematically shown in Fig. 2(c). The –C–N stretching vibrations and –C–H bending vibrations are indicated with "+" and "*" for pure PVP and nanocomposite in Fig. 2.

3.3. TGA analysis

The thermal stability was determined by thermogravimetric analysis (TGA, PerkinElmer Instruments model, STA 6000). The TGA thermograms were recorded for 5 mg of powder sample at a heating rate of 10 K min^{-1}. in the temperature range of 303–1073 K under nitrogen atmosphere. To further confirm the existence of PVP on the surface of Mn_3O_4 nanoparticles and quantify the proportion of organic and inorganic phase, TGA was performed in the temperature range of 303–973 K; thermograms and differential thermograms are given in Fig. 3. Pure PVP combusted starting at ~703 K leaving a residue of ~1–2% above 773 K (Fig. 3(a)). Evidently, the differential thermogram for the nanocomposite is slightly shifted towards higher temperatures due to the extra interaction between the PVP and nanoparticles [22,23]. Nanocomposite shows a major weight loss of 55% over the temperature range of 303–973 K due to the decomposition and combustion of PVP (Fig. 3(b)). This implies that nanocomposite has ~45% inorganic phase as Mn_3O_4 nanoparticles.

3.4. TEM analysis

Transmission electron microscopy (TEM) analysis was performed using a FEI Tecnai G2 Sphera microscope. A drop of diluted sample in alcohol was dripped on a TEM grid.

Morphology and size distribution of the nanoparticles in the nanocomposite was analyzed using TEM. Few micrographs and histogram calculated thereof are presented in Fig. 4. Polymer is invisible in TEM as no staining has been used to make them visible. Mn_3O_4 particles exhibit near spherical morphology and seem to be single crystalline as indicated by Fig. 4(b). Average size for the

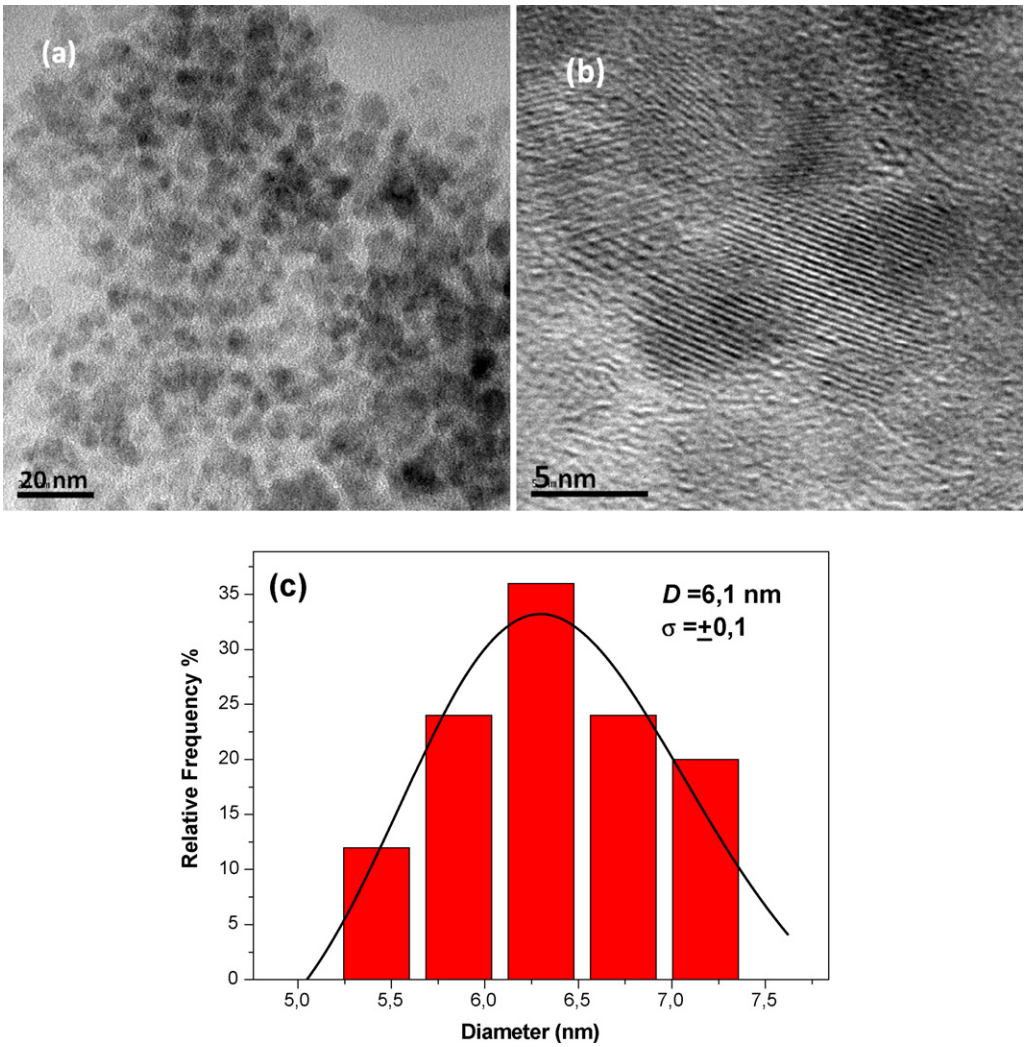

Fig. 4. (a and b) TEM micrographs of PVP–Mn_3O_4 nanocomposite at different magnifications; and (c) calculated histogram from several TEM images with a log-normal fitting.

Mn_3O_4 nanoparticles, calculated by log-normal fitting to the size distribution histogram, was obtained as 6.1 ± 0.1 nm. As compared with the crystallite size from X-ray line profile fitting, this reflects dominantly single crystalline nature of the Mn_3O_4 nanoparticles in the nanocomposite.

3.5. VSM analysis

VSM measurements were performed by using a Quantum Design Vibrating sample magnetometer (QD-VSM). The sample was measured between ±10 kOe at room temperature and 10 K. ZFC (zero-field cooling) and FC (field cooling) measurements were carried out at 100 Oe and the blocking temperature was determined from the measurements. To investigate the magnetic properties in PVP–Mn_3O_4 nanocomposite, the magnetization in both zero-field-cooled (ZFC) and field-cooled (FC) modes under 100 Oe magnetic field were measured. ZFC measurement was carried out under cooling to 10 K without any applied external magnetic field. Then 50 Oe magnetic field was applied during the heating of sample. The FC and ZFC curves are coincident and spin in PVP–Mn_3O_4 nanocomposite aligned randomly as in paramagnetic systems above 42 K. The temperature at which spins' alignment change from ordered to random is known as T_C, and is determined as 42 K for PVP–Mn_3O_4 nanocomposite with average Mn_3O_4 particle size of 6 nm. Our results are in agreement with T_C reported for Mn_3O_4 by Winkler et al. [24] and Regmi et al. [25] as 42 K for particle with 15 nm average size. The bulk Mn_3O_4 has curie temperature of about 42 K [26].

In the ZFC curve (Fig. 5) the magnetization started to increase sharply at 42 K with decreasing temperature until 35 K, it reached a

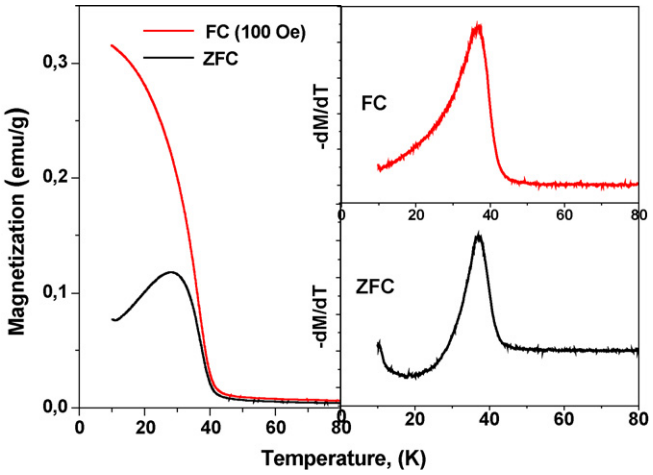

Fig. 5. Zero-field-cooled (ZFC) and field-cooled (FC) magnetization curves for polyol synthesized PVP–Mn_3O_4 nanocomposite measured at 100 Oe external magnetic field, and $-dM/dT$ curves with respect to temperature for both FC and ZFC.

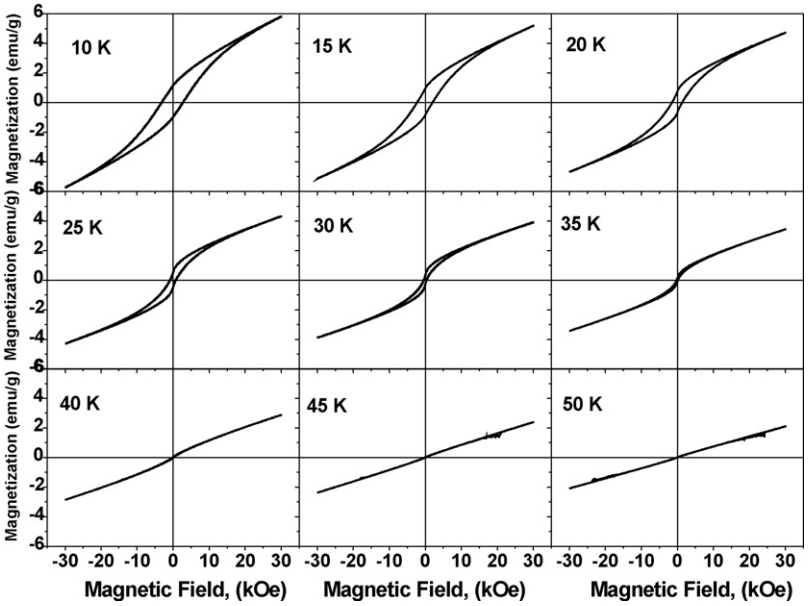

Fig. 6. Magnetization (M) as a function of external magnetic field (H) at different temperatures for polyol synthesized PVP–Mn_3O_4 nanocomposite.

maximum value at 28.5 K where the thermal energy became comparable with the anisotropy energy and then decreased suddenly, revealing the blocking temperature, T_B. A detailed study on magnetic transition temperatures for 15–25 nm Mn_3O_4 nanoparticles can be found in Refs. [24,25]. The opposite sign of first derivatives of magnetization with respect to elevated temperatures verifies the magnetic phase transition at about 42 K. This first derivative characteristics are similar to that reported by Winkler et al. [24]. There are two reported anomalies [27,28] in temperature dependent magnetic characteristic in Mn_3O_4 below main magnetic phase transition at 42 K. These are at 32 K and 39 K and were attributed to the spin reorientations with the resultant ESR experiments in Ref. [27]. However, we investigate these magnetic phase transitions at 28.5 K and 35 K for these anomalies.

The magnetic hysteresis loops of the PVP–Mn_3O_4 nanocomposite are shown in Fig. 6 at different temperature below and above T_B in a magnetic field up to ±30 kOe. The saturation magnetization (M_S) was not reached, showing a maximum of magnetization (M_{max}) at about 9.5 emu/g at 10 K. As the normalization of M_S was made against the total nanocomposite weight, the obtained value is lower than that of bulk Mn_3O_4 [26,29]. Considering inorganic content of 45% and normalizing against this weight a value of ~21 emu/g Mn_3O_4 was obtained where the bulk M_S is 38 emu/g [5,30].

This non-saturated hysteresis can be attributed to the coexistence of antiferromagnetic interactions with ferromagnetic interaction tending to saturate at low temperatures. The sample has hysteresis with small coercivity (H_C) and remanent magnetization (M_r) at 40 K which is in closer conditions to the superparamagnetic state. The superparamagnetic PVP–Mn_3O_4 nanocomposite has giant core magnetic moment that tends to be aligned with field, and canted spins with non-aligned tendency at the surface at about 40 K. Additionally, the size distribution which allows the existence of some particles below the threshold diameter (7 nm) for single domain Mn_3O_4 NP's and the temperature gradient during cooling may cause the superparamagnetic like characteristic at 40 K. The magnetic hysteresis loops the T_C for PVP–Mn_3O_4 nanocomposites show paramagnetic trend with linear M with respect to H as expected. All hysteresis show a small amount of asymmetric coercive field and this asymmetry is increasing with decreasing temperature.

Fig. 7 shows the temperature dependence of the H_C, M_r and M_S predicted from extrapolation of M vs. $1/H$ plots. The H_C decreases by increasing temperature and becomes zero above T_C. The M_S has decreasing concave down curve and also the M_r, characteristic of ferrimagnetic states, decreases. However, it has sharp decrease when the temperature gets closer to the T_C. It can be inferred that

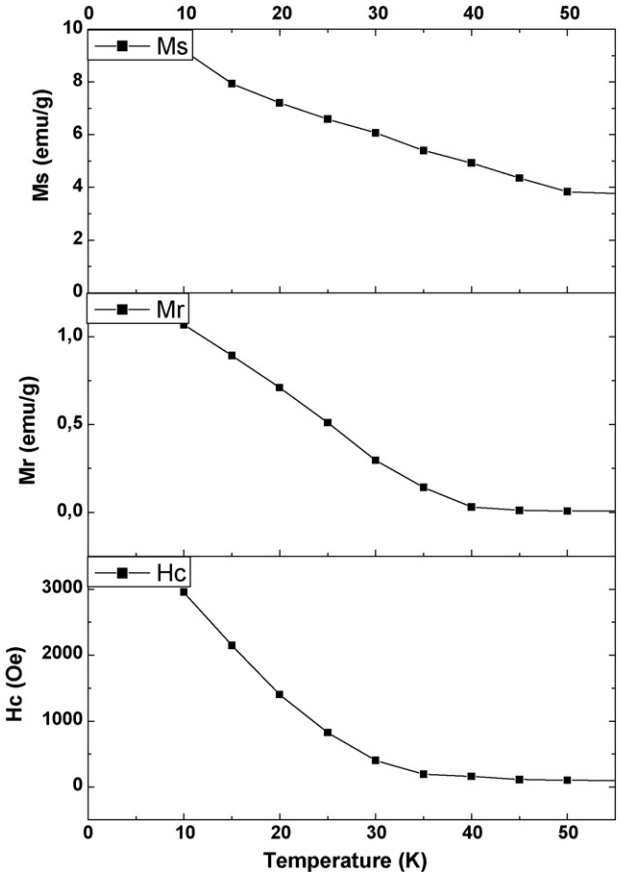

Fig. 7. Temperature dependence of H_C, M_r and M_S for polyol synthesized PVP–Mn_3O_4 nanocomposite.

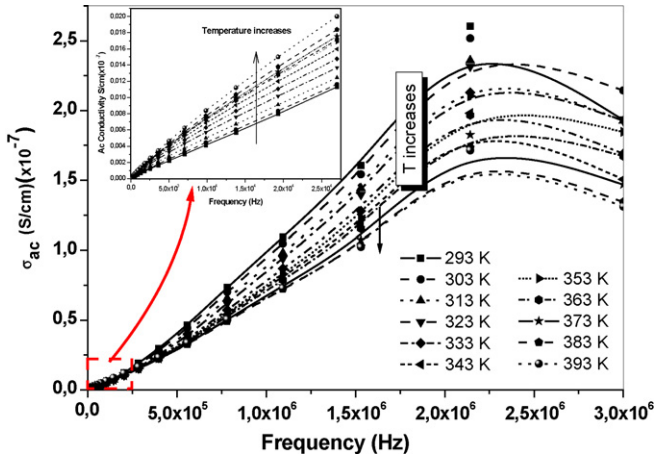

Fig. 8. ac conductivities vs. frequency of pure PVP at temperatures ranging from RT to 393 K.

this relation between M_S and M_r shows the phase transition at about T_C.

3.6. Conductivity and dielectric measurements

The real (ε') and imaginary (ε'') parts of complex dielectric permittivity $\varepsilon^*[= \varepsilon'(\omega) + i\varepsilon''(\omega)]$ were measured with a Novocontrol dielectric-impedance analyzer. The dielectric data (ε', ε'') were collected during heating as a function of frequency. The films were sandwiched between gold blocking electrodes and the conductivities were measured in the frequency range 0.1 Hz to 1 MHz at 283 K intervals. The temperature was controlled with a Novocontrol cryosystem, between 173 and 523 K.

3.6.1. Conductivity measurements

The ac conductivity, σ_{AC}, of pure PVP and PVP–Mn_3O_4 nanocomposite is presented in Figs. 8 and 9. Initially, ac conductivity of pure PVP sample is almost linearly dependent on frequency of up to 2 MHz. However, at low frequencies ranging from 0 KHz to 3 KHz, as shown in the inset of Fig. 8, the degree of frequency-dependency increases with temperature while at the medium frequencies between 3 KHz and 2 MHz it increases with decreasing temperature. The ac conductivity decreases with the frequency after peaking at around 2.1 MHz. At high frequency, the ac conductivity becomes more complicated with the temperature increment. This type of dependency in this range seems to be unclear to us at the moment or this might be the initiation of the tunelling of electronic transportation through the capacitively coupled nanoparticles. However, at low and medium frequency range, the ac conductivity of pure PVP polymer generally obeys Jonscher's power law [31] as

$$\sigma(f) = \sigma(0)\left[1 + \left(\frac{f}{f_r}\right)^n\right]$$

where $\sigma(0)$ is the dc conductivity f and f_r are the applied frequency and relaxation frequency, respectively; n is an exponent which is slightly less than unity, and additionally is slightly dependent to the variation of temperature between RT and 393 K, $\sigma(0)f_r^{0.95} = 1.05 \times 10^{-6}$ for this experiment. The frequency-dependent conductivity mechanism of the PVP polymer leads to both diffusive below partly relaxation frequency and subdiffusive motion of mobile charges, giving rise to dispersion in the conductivity. The effect of both diffusive and subdiffusive conductivities is relevant to the temperature dependency as shown in Fig. 8 together with the inset.

The nanostructures of binary composites like the combination of conductor–insulator arrays usually have some basic rules. The first is the matrix formation in which the nanoparticles or nanocrystallites are embedded and always capped by the matrix materials, which can be either conductor capped by insulator or vice versa. So there will be no identical nanoparticle contacts among them. In this case the dc and ac conductivity is usually described by the Maxwell–Wagner model [32]. The second is the percolation formation, which can be considered to be constructed by randomly packing the two types of nanoparticles together. In percolation system, there exists a critical volume fraction above which the electrical properties are dominated by the conducting component and below which the insulating component dominates.

The PVP–Mn_3O_4 nanocomposite has strongly frequency-dependent conductivity behaviour. Within the general tendencies of the ac conductivity, it resembles to the electrical characterisation of the pure PVP polymer. At low frequency it increases with temperature as shown in the inset of Fig. 9 while frequency-dependent conductivity increases with decreasing temperature over 3 KHz. This attitude can be explained by the models mentioned above. Generally, Mn_3O_4 has a conductivity in the order of 10^{-5} S cm^{-1} at lower frequencies. The ac conductivity changes with respect to frequency can be explained by electronic exchange occurring between Mn^{+2} and Mn^{+3} existing in sublattice of spinel lattice. At lower frequencies this exchange can not be observed, but at higher frequencies the electronic exchange can follow the ac source.

The temperature dependency of the conductivity of PVP–Mn_3O_4 shown in Figs. 9 and 10 seems to be quite small, as also illustrated in the TGA thermograms measured in the temperature range of 293–393 K, while its frequency-dependency is found to be quite high. At lower temperatures, the σ_{ac} slightly increases and then decreases with a small hill, but it increases linearly with increasing temperature above 333 K. This wide, small hill at lower temperatures vanishes at moderate frequencies and conductivity increases linearly by increasing elevated temperatures. At highest frequencies, the composite has decreasing conductivity than increase again upon heating. There is no expected change in the composite to cause the observed changes in conductivity, but the expulsion of water during heating can cause the change in conductivity.

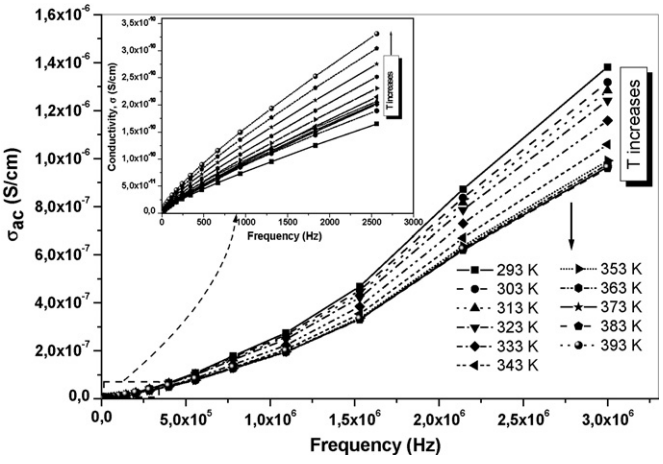

Fig. 9. ac conductivity vs. frequency for PVP–Mn_3O_4 nanocomposite at temperatures ranging from RT to 393 K.

3.6.2. Dielectric measurements

The complex permittivity parameters $\varepsilon = \varepsilon' + i\varepsilon''$, were measured to determine the frequency and temperature dependency of stored (ε') and dissipated energies (ε'') by PVP–Mn_3O_4 nanocomposite and results are presented in Fig. 11(a) and (b). The real part of the permittivity decreases by increasing frequency at various temperatures, while imaginary part decreases first and than increases at higher frequencies. The inset of Fig. 11(b) shows that imaginary

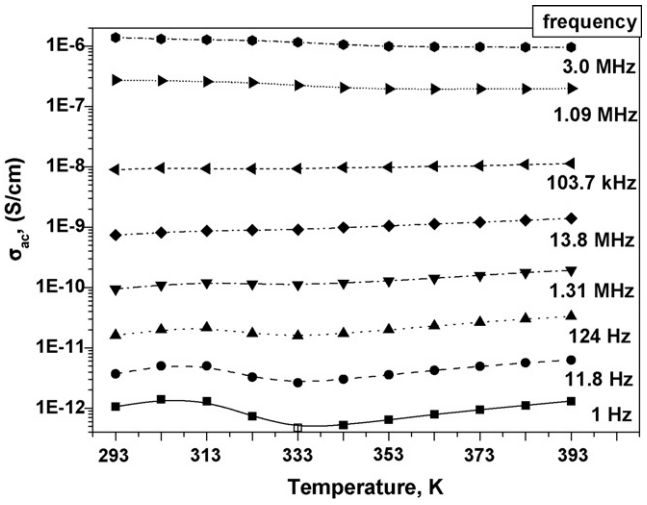

Fig. 10. ac conductivities vs. temperatures of PVP–Mn_3O_4 nanocomposite for frequencies ranging from 1 Hz to 3 MHz.

part is fluctuating and increasing as a function of temperature for the lower frequency and than decreases for higher frequencies. This means that the temperature dependency of the imaginary part is strongly dependent on the frequency range. Furthermore, the real part shows the similar manners as depicted in the inset of Fig. 11(a), however, it reduces with the increase in frequency. It is worthy to note that its temperature dependency for all the frequency range studied here except for very low frequency, which can be considered to be a dc response, remains almost unchanged. Koop's theory, based on the Maxwell–Wagner model for the homogeneous double structure [32], is generally used to explain the dielectric characteristic of semiconductor like spinel structures such as ferrites. In double structure model, the highly conducting grains are separated by relatively poor conducting grain boundaries and are found to be more effective at higher frequencies, while grains are more effective at lower frequencies [33]. The conductivity difference between grains and grain boundaries means different resistance causing the accumulation of charge carriers in separated boundaries and increase in dielectric constants. The polarization in Mn_3O_4 is through a mechanism similar to the conduction process by electron exchange between Mn^{2+} and Mn^{3+}, the local displacement of electrons in the direction of the applied field occurs and these electrons determine the polarization. With increasing frequency, the polarization decreases and reaches to a constant value due to the electron exchange between Mn^{2+} and Mn^{3+} cannot follow the alternating field. Previously, the large value of dielectric constant at lower frequency was attributed to the predominance of species like Mn^{2+} ions, oxygen vacancies, grain boundary defects as in ferrites [34]. The decrease in dielectric constant with frequency is natural because of the fact that any species contributing to polarizability is found to show lagging behind the applied field at higher frequencies [32]. The curves for both the real and imaginary parts of PVP–Mn_3O_4 as a function of frequency are found to be slightly temperature dependent, except for very low frequencies. By the very small size of particles sublattice structure of spinel phase is destroyed at the surface and both the dielectric relaxations of real and imaginary part show nearly same characteristics at elevated temperatures by varying frequency.

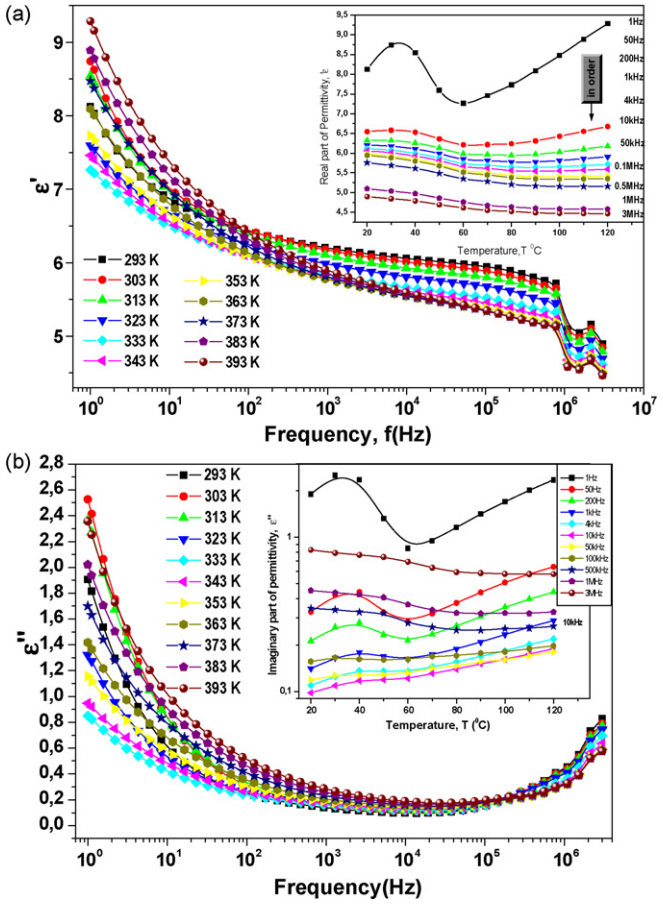

Fig. 11. (a) Real and (b) imaginary parts of permittivity of PVP–Mn_3O_4 nanocomposite as a function of frequency at various temperatures.

4. Conclusion

PVP–Mn_3O_4 nanocomposites were successfully synthesized via a polyol route and evaluated for their structural, magnetic and dielectric properties. A surfactant-free single step solvothermal route was successfully utilized to produce crystalline Mn_3O_4 nanoparticles with high purity and uniformity. Crystalline phase, identified as Mn_3O_4 were found to exhibit an average crystallite size of 6 ± 1 nm from X-ray line profile fitting and an average particle size of 6.1 ± 0.1 nm from TEM analysis. These particles show nearly single crystalline nature. The interaction between PVP and Mn_3O_4 nanoparticles was confirmed by FT-IR spectroscopy, being via bridging oxygens of the carbonyl (C=O) and the nanoparticle surface. T_C and T_B for the nanocomposite were observed at 42 K and 28.5 K, respectively. The sample has hysteresis with small H_C and M_r at 40 K, resembling the superparamagnetic state. Conductivity measurements on PVP–Mn_3O_4 nanocomposite revealed a σ_{ac} in the order of 10^{-7} S cm^{-1} at lower frequencies. The σ_{ac} changes with respect to frequency can be explained by electronic exchange occurring between Mn^{+2} and Mn^{+3} existing in sublattice of spinel lattice. The ε' and ε'' of PVP–Mn_3O_4 as a function of frequency are found to be slightly temperature dependent.

Acknowledgements

The authors are thankful to the Fatih University, Research Project Foundation (Contract no: P50020803-2) and Turkish Ministry of Industry and Trade (Contract no: 00185.STZ.2007-2) for financial support of this study. MST acknowledges the fellowship from Knut and Alice Wallenbergs Foundation (No: UAW2004.0224).

References

[1] Y.F. Shen, R.P. Zerger, R.N. DeGuzman, S.L. Suib, L. McCurdy, D.I. Potter, C.L. O'Young, Science 260 (1993) 511.

[2] D.K. Kim, M.S. Amin, S. Elborai, S.H. Lee, Y. Koseoglu, M. Zahn, M. Muhammed, J. Appl. Phys. 97 (2005) 10J510.
[3] A.R. Armstrong, P.G. Bruce, Nature 381 (1996) 499.
[4] T. Özkaya, A. Baykal, M.S. Toprak, Cent. Eur. J. Chem. 6 (3) (2008) 465.
[5] T. Ozkaya, A. Baykal, H. Kavas, Y. Köseoğlu, M.S. Toprak, Physica B 403 (2008) 3760.
[6] Z. Durmuş, H. Kavas, A. Baykal, M.S. Toprak, Cent. Eur. J. Chem. 7 (3) (2009) 555.
[7] Z. Durmuş, A. Baykal, H. Kavas, M. Direkçi, M.S. Toprak, Polyhedron 28 (2009) 2119.
[8] Y.Q. Chang, X.Y. Xu, X.H. Luo, C.P. Chen, D.P. Yu, J. Cryst. Growth 264 (2004) 232.
[9] Z.Y. Chang, T. Qiao, X.Y. Hu, J. Solid State Chem. 177 (2004) 4093.
[10] E. Finocchio, G. Busca, Catal. Today 70 (2001) 213.
[11] S.K. Apte, S.D. Naik, R.S. Sonawane, B.B. Kale, N. Pavaskar, A.B. Mandale, B.K. Das, Mater. Res. Bull. 41 (2006) 647.
[12] S.K. Apte, S.D. Naik, R.S. Sonawane, B.B. Kale, N. Pavaskar, A.B. Mandale, B.K. Das, Mater. Res. Bull. 41 (3) (2006) 647.
[13] Z.W. Chen, J.K.L. Lai, C.H. Shek, Scripta Mater. 55 (2006) 735.
[14] F. Fievet, J.P. Lagier, B. Blin, B. Beaudoin, M. Figlarz, Solid State Ionics 32–33 (1989) 198.
[15] C. Feldman, G.O. Jungk, Angew. Chem. Int. Ed. 40 (2001) 359.
[16] W. Cai, J. Wan, J. Colloid Interface Sci. 305 (2007) 366.
[17] T. Wejrzanowski, R. Pielaszek, A. Opalinska, H. Matysiak, W. Łojkowski, K.J. Kurzydłowski, Appl. Surf. Sci. 253 (2006) 204.
[18] R. Pielaszek, in: Proceedings of the XIX Conference, Krakow, Poland, Appl. Crystallogr. (2003), pp. 43.
[19] A. Baykal, Y. Köseoğlu, M. Şenel, Cent. Eur. J. Chem. 5 (1) (2007) 169.
[20] G.G. Couto, J.J. Kleinb, W.H. Schreiner, D.H. Mosca, A.J.A. de Oliveira, A.J.G. Zarbin, J. Colloid Interface Sci. 311 (2007) 461.
[21] J.D. Patel, T.K. Chaudhuri, Mater. Res. Bull. 44 (2009) 1647.
[22] Y. Xiaotun, X. Lingge, N.S. Choon, C.S. Hardy, Nanotechnology 14 (2003) 624.
[23] Z.J. Zhang, X.Y. Chen, B.N. Wang, C.W. Shi, J. Cryst. Growth 310 (2008) 5453.
[24] E. Winkler, R.D. Zysler, D. Fiorani, Phys. Rev. B 70 (2004) 174406.
[25] R. Regmi, R. Tackett, G. Lawes, J. Magn. Magn. Mater. 321 (2009) 2296.
[26] A.V. Olmos, R. Redón, G.R. Gattorno, M.E. Mata-Zamora, F. Morales-Leal, A.L. Osorio, J.M. Saniger, J. Colloid Interface Sci. 291 (2005) 175.
[27] G. Srinivasan, M.S. Seehra, Phys. Rev. 28 (1983) 1.
[28] A. Baykal, H. Kavas, Z. Durmus, M. Demir, S. Kazan, R. Topkaya, M.S. Toprak, Cent. Eur. J. Chem. 8 (3) (2010) 633.
[29] R.S. Tebble, D.J. Craik, Magnetic Materials, Academic Press, New York, 1969, p. 993.
[30] D. Fiorani, S. Vitiocoli, J.L. Dorman, J.L. Tholence, A.P. Murani, Phys. Rev. B 30 (1984) 2776.
[31] J. Glass, P. Poddar, J. Almand, S. Srinath, H. Srikanth, Adv. Funct. Mater. 16 (2006) 71.
[32] A.M.M. Farea, S. Kumar, K.M. Batoo, J. Alloys Compd. 464 (2008) 361.
[33] V.L.G. Uitert, Proc. IRE 44 (1956) 1294.
[34] W. Li, H.L. Wang, J. Am. Chem. Soc. 126 (8) (2004) 2278.